nature geoscience

LETTERS

PUBLISHED ONLINE: 8 JANUARY 2012 | DOI: 10.1038/NGEO1358

Determining the natural length of the current interglacial

P. C. Tzedakis[1]*, J. E. T. Channell[2], D. A. Hodell[3], H. F. Kleiven[4,5] and L. C. Skinner[3]

No glacial inception is projected to occur at the current atmospheric CO_2 concentrations of 390 ppmv (ref. 1). Indeed, model experiments suggest that in the current orbital configuration—which is characterized by a weak minimum in summer insolation—glacial inception would require CO_2 concentrations below preindustrial levels of 280 ppmv (refs 2–4). However, the precise CO_2 threshold[4–6] as well as the timing of the hypothetical next glaciation[7] remain unclear. Past interglacials can be used to draw analogies with the present, provided their duration is known. Here we propose that the minimum age of a glacial inception is constrained by the onset of bipolar-seesaw climate variability, which requires ice-sheets large enough to produce iceberg discharges that disrupt the ocean circulation. We identify the bipolar seesaw in ice-core and North Atlantic marine records by the appearance of a distinct phasing of interhemispheric climate and hydrographic changes and ice-rafted debris. The glacial inception during Marine Isotope sub-Stage 19c, a close analogue for the present interglacial, occurred near the summer insolation minimum, suggesting that the interglacial was not prolonged by subdued radiative forcing[7]. Assuming that ice growth mainly responds to insolation and CO_2 forcing, this analogy suggests that the end of the current interglacial would occur within the next 1500 years, if atmospheric CO_2 concentrations did not exceed 240 ± 5 ppmv.

The notion that the Holocene (or Marine Isotope Stage 1, MIS1), already 11.6 thousand years (kyr) old, may be drawing to a close has been based on the observation that the duration of recent interglacials was approximately half a precession cycle (~11 kyr; ref. 8). However, uncertainty over an imminent hypothetical glaciation arises from the current subdued amplitude of insolation variations as a result of low orbital eccentricity (Fig. 1). It has thus been proposed that at times of weak eccentricity–precession forcing, obliquity is the dominant astronomical parameter driving ice-volume changes, leading to extended interglacial duration of approximately half an obliquity cycle (~21 kyr; ref. 9). In this view, the next glacial inception would occur near the obliquity minimum ~10 kyr from now[7].

Climate modelling studies show that a reduction in boreal summer insolation is the primary trigger for glacial inception, with CO_2 playing a secondary role[3,5]. Lowering CO_2 shifts the inception threshold to higher insolation values[1], but modelling experiments indicate that preindustrial concentrations of 280 ppmv would not be sufficiently low to lead to new ice growth given the subdued insolation minimum[2–4]. However, the extent to which

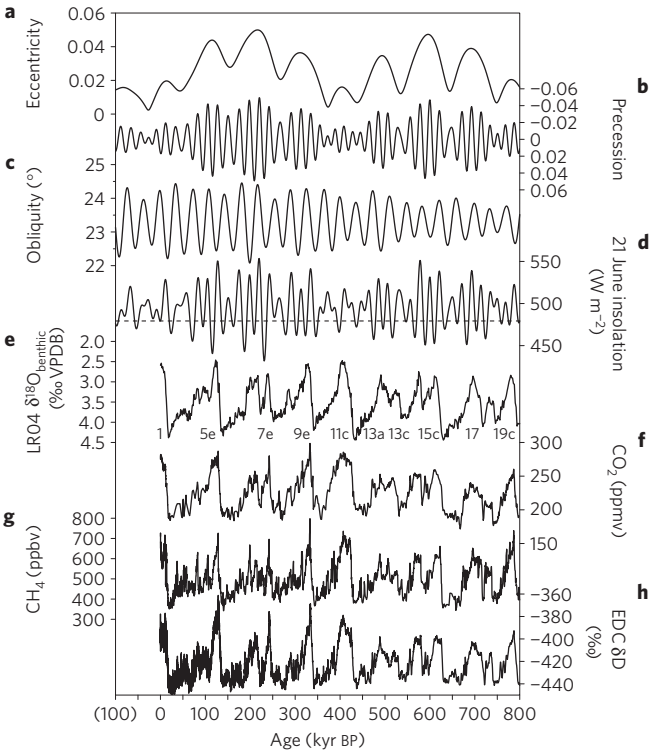

Figure 1 | Astronomical parameters 100 kyr after present—800 kyr BP and palaeoclimatic records 0–800 kyr BP. a, Eccentricity[29]; **b**, precession index, plotted on an inverse vertical axis[29]; **c**, obliquity[29]; **d**, 21 June insolation 65° N (ref. 29); **e**, $\delta^{18}O_{benthic}$ record from the LR04 stack[28]; **f**, atmospheric CO_2 concentration in Antarctic ice cores[12]; **g**, atmospheric CH_4 concentration in the Antarctic EDC ice core[13]; **h**, δD composition of ice in the EDC ice core[18]. Marine Isotopic Stages and sub-Stages corresponding to interglacials are indicated. Ages in parentheses denote years after present. The dashed line indicates the current 21 June insolation level at 65° N.

preindustrial CO_2 levels were 'natural' has been challenged[10,11] by the suggestion that anthropogenic interference since the mid-Holocene led to increased greenhouse gas (GHG) concentrations, which countered the natural cooling trend and prevented a glacial inception. The overdue glaciation hypothesis has been tested by climate simulations using lower preindustrial GHG concentrations,

[1]Environmental Change Research Centre, Department of Geography, University College London, London WC1E 6BT, UK, [2]Department of Geological Sciences, University of Florida, Gainesville, Florida 36211, USA, [3]Department of Earth Sciences, University of Cambridge, Cambridge CB2 3EQ, UK, [4]Department of Earth Science and the Bjerknes Centre for Climate Research, University of Bergen, N-5007 Bergen, Norway, [5]UNI Research AS, N-5007 Bergen, Norway. *e-mail: p.c.tzedakis@ucl.ac.uk.

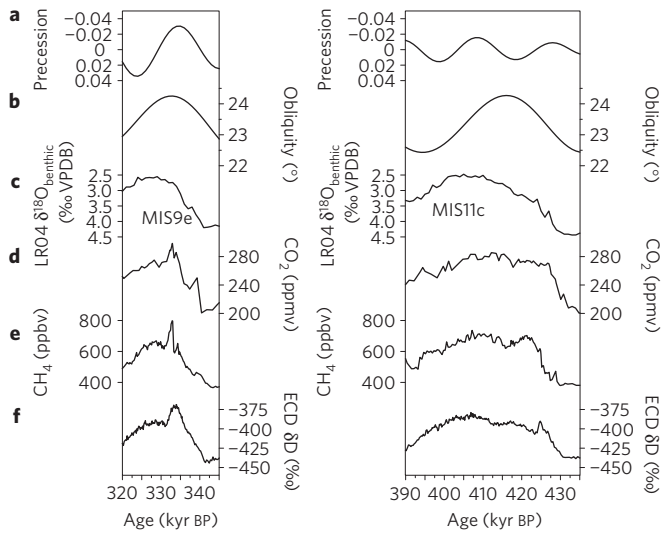

Figure 2 | Two types of interglacial according to structure: MIS9 and MIS11. a, Precession index, plotted on an inverse vertical axis[29]; **b**, obliquity[29]; **c**, $\delta^{18}O_{benthic}$ record from the LR04 stack[28]; **d**, atmospheric CO_2 concentration in Antarctic ice cores[12]; **e**, atmospheric CH_4 concentration in the EDC ice core[13]; **f**, δD composition of ice in the EDC ice core[18].

with contrasting results, ranging from no ice growth[5] to a linear increase in ice volume[4] to large increases in perennial ice cover[6].

Empirical evidence from intervals characterized by similar boundary conditions to the current interglacial may also be used to infer the timing of the next 'natural' glacial inception, assuming that, for a given insolation and CO_2 forcing, ice-volume responses between two periods are also similar. Here, we limit the search for potential Holocene analogues to the past 800 kyr, for which ice-core records of atmospheric GHG concentrations are available[12,13]. We then explore approaches to constraining the timing of glacial inception and assess the relevance of this information to the current interglacial.

Interglacials may be described in terms of their intensity, structure and astronomical signature (Fig. 1). With respect to intensity, interglacials preceding the Mid-Brunhes Event (MBE: 430 kyr before present, BP) are characterized by reduced CO_2 concentrations, cooler Antarctic temperatures and greater benthic foraminiferal oxygen isotope ($\delta^{18}O_{benthic}$) values[14]. The latter may point to lower-than-present sea-level highstands, but they may instead reflect lower deep-water temperatures. Lower pre-MBE interglacial intensities are not observed in certain Eurasian records[14].

With respect to structure, two broad categories (Fig. 2) emerge: (1) MIS5e, MIS7e, MIS9e and MIS19c are characterized by rapid deglaciation, early peaks in Antarctic temperatures and GHG concentrations followed by monotonic declines; and (2) MIS11c and MIS17 are characterized by protracted deglaciation[11,15] and the persistence of interglacial values over two insolation peaks, with the obliquity maximum post-dating the first precession minimum by 12–13 kyr and preceding the second precession minimum by 8 kyr. MIS1 shares some characteristics of the first group, but the early peaks in Antarctic temperatures and GHG concentrations were not followed by monotonic declines. Two 'rogue' interglacials are not included under these categories. MIS13c was preceded by a minor glaciation, and maximum warming was reached in MIS13a. MIS15c has many similarities with MIS1 (Supplementary Fig. S1): the precession minimum occurred near the obliquity maximum, Antarctic temperatures peaked early and then remained stable and CO_2 concentrations rose gradually throughout the interglacial. However, MIS15c is

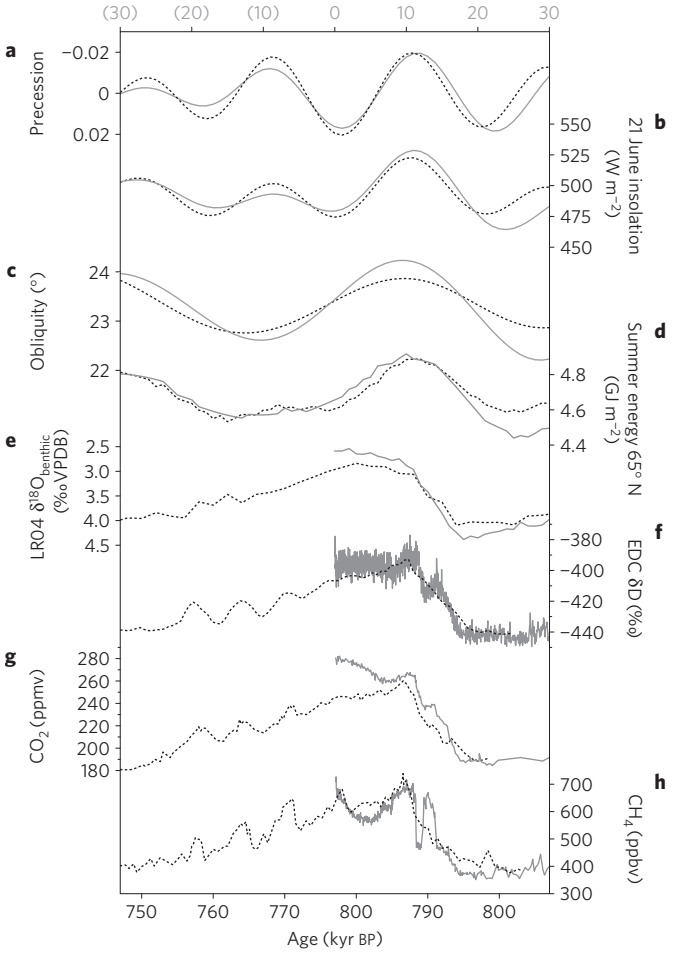

Figure 3 | Alignment of the past and future 30 kyr (grey line) and a 60-kyr interval encompassing MIS19 (dotted line). a, Precession index, plotted on an inverse vertical axis[29]; **b**, 21 June insolation at 65° N (ref. 29); **c**, obliquity[29]; **d**, summer energy at 65° N, defined as the sum of the diurnal average insolation on days exceeding 300 W m^{-2} (ref. 30); **e**, $\delta^{18}O_{benthic}$ record from the LR04 stack[28]; **f**, δD composition of ice in the EDC ice core[18]; **g**, atmospheric CO_2 concentration in Antarctic ice cores[12]; **h**, atmospheric CH_4 concentration in the EDC ice core[13]. Ages in parentheses denote years after present.

characterized by a slow deglaciation[11], indicating that the analogy with MIS1 has its limitations.

In terms of astronomical signature, only MIS11c and MIS19c are comparable to the Holocene as a result of weak eccentricity–precession forcing. MIS11c has traditionally been considered a close astronomical analogue for the Holocene[2], but differences in the phasing of precession and obliquity have led to different alignments of the two intervals, with contrasting implications for the natural length of the current interglacial[2,9,10,16]. Alignment ambiguities and differences in deglaciation trajectories[11,15,17], therefore, impose limitations on the MIS1–MIS11c analogy. By contrast, the obliquity maximum occurs very near the precession minimum in both MIS1 and MIS19c, although absolute values of obliquity are different (Fig. 1). Thus, alignment of the two intervals is unambiguous, with today corresponding to ~777 kyr BP (ref. 17; Methods). Comparison of MIS1 and MIS19c (Fig. 3) reveals many similarities in their palaeoclimatic signals, although their CO_2 trajectories diverge. Given its astronomical configuration and deglaciation history, MIS19c seems sufficiently similar to MIS1 to warrant comparisons.

In theory, if the analogy with MIS1 is correct and ice growth mainly responds to insolation and CO_2 forcing, the duration of

MIS19c could provide an indication as to when the hypothetical end of the current interglacial might be expected. In practice, constraining the timing of glacial inception during MIS19 is not straightforward because direct sea-level determinations are unavailable and $\delta^{18}O_{benthic}$ may be overprinted by local deep-water temperature and hydrographic effects. Although pinpointing the onset of new ice growth is difficult, an indication of the presence of ice-sheets is provided by millennial-scale variability characterized by a distinct pattern of interhemispheric phasing. During the last glacial, iceberg discharges into the North Atlantic are widely believed to have disrupted the Meridional Overturning Circulation (MOC), leading to rapid cooling of the North Atlantic and gradual warming of Antarctica. Reactivation of the MOC led to gradual Antarctic cooling as Greenland warmed abruptly[18]. This asynchronous phasing can be explained by a bipolar-seesaw mechanism[19], whereby changes in the strength of the MOC lead to changes in interhemispheric heat transport. An asymmetric response has also been observed in North Atlantic cores on the Portuguese margin[20,21] and the Gardar Drift[22], where $\delta^{18}O_{planktonic}$ records resemble Greenland temperature records, reflecting rapid migration of the polar front[20], whereas $\delta^{18}O_{benthic}$ curves resemble Antarctic temperature records, in both shape and phasing relative to surface-water changes. This primarily reflects changes in local deep-water $\delta^{18}O_{dw}$, largely attributed to changes in deep-water sourcing and/or source signature[23].

We propose that the onset of bipolar-seesaw variability provides a minimum age for glacial inception. This can be tested by examining the last glacial inception, the only relevant period with direct sea-level determinations and precise chronologies. At the MIS5e–5d transition, the first major perturbation of the MOC occurred during cold-water event C24, characterized by abrupt surface cooling, gradual decrease in $\delta^{18}O_{benthic}$ values and ice-rafting in the North Atlantic, and gradual warming in Antarctica (Supplementary Fig. S2 and references). Sea level started falling monotonically between 115 and 113 kyr BP (ref. 24), reaching 20–30 m below present by the time of event C24. This occurred ~111 kyr BP according to revised estimates based on precisely dated speleothem records, lagging glacial inception by ~3 kyr (Supplementary Fig. S3 and references).

With respect to MIS19, three lines of evidence indicate the onset of bipolar-seesaw behaviour: ice-core data, phasing of benthic–planktonic $\delta^{18}O$ signals and appearance of ice-rafted detritus (Fig. 4). At the MIS19c–19b transition, the EPICA Dome C (EDC) Antarctic ice core shows three well-defined peaks in δD_{ice}, CO_2 and CH_4 values[12,13]. The amplitudes and relative rates of change between these records are similar to those observed in the last glacial[12]. By contrast, an earlier peak in CH_4 around 778 kyr BP is not associated with δD_{ice} or CO_2 changes. In the marine realm, three distinct oscillations in $\delta^{18}O_{planktonic}$ values are also recorded during the MIS19c–19b transition in Ocean Drilling Program (ODP) site 983 in the Gardar Drift[25,26]. Minima in $\delta^{18}O_{planktonic}$ are phase-shifted relative to $\delta^{18}O_{benthic}$ decreases, in a manner similar to MIS3 changes[26,27]. Cross-correlation analysis (Methods) shows that the highest correlation is obtained with $\delta^{18}O_{benthic}$ leading $\delta^{18}O_{planktonic}$ by 950 years during MIS19 in ODP 983 and 822–950 years during MIS3 in Portuguese margin sequences[20,21], supporting the hypothesis of a common underlying mechanism between the two periods. Finally, the appearance of ice-rafted detritus (ref. 26) at the onset of asynchronous phasing between benthic and planktonic $\delta^{18}O$ suggests that ice-sheets had become large enough to calve along coastlines and disrupt the MOC. The onset of these changes, at 772.5 kyr BP in the EDC3 chronology and 774.5 kyr BP in ODP 983 (Methods), has been stratigraphically linked through the position of the Matuyama–Brunhes palaeomagnetic boundary identified in both cores[27].

In MIS19, the onset of bipolar-seesaw variability post-dates the minimum in boreal summer insolation by 2.5–4.5 kyr. However, the length of time between new ice growth and the onset

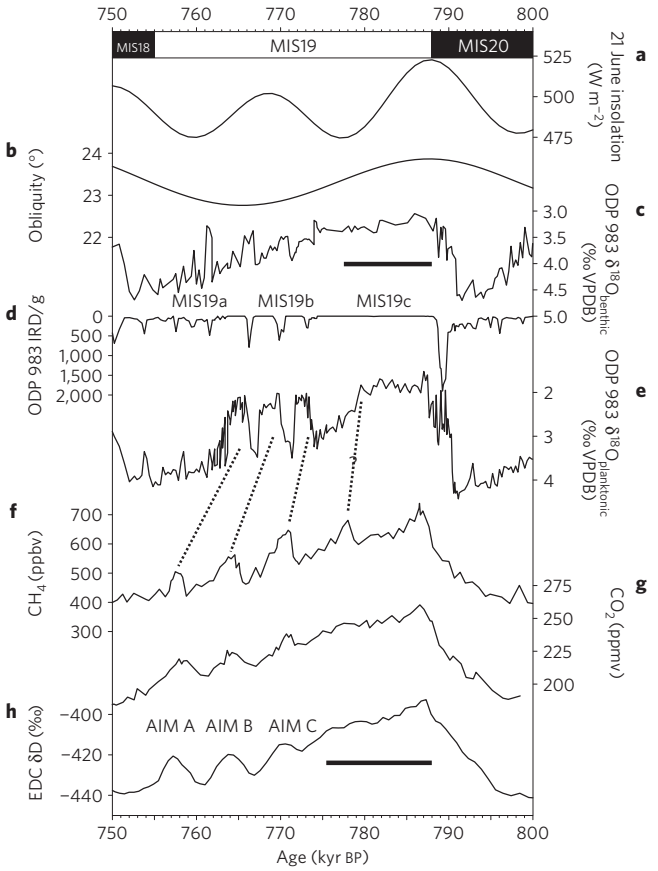

Figure 4 | MIS19 palaeoclimatic records. a, 21 June insolation at 65° N (ref. 29); **b** obliquity[29]; **c**, $\delta^{18}O_{benthic}$ record from ODP 983 (ref. 25); **d**, ODP 983 ice-rafted detritus (IRD) content (numbers per gram)[26]; **e**, $\delta^{18}O_{planktonic}$ record from ODP 983 (ref. 25); **f**, atmospheric CH_4 concentration in the EDC ice core[13]; **g**, atmospheric CO_2 concentration in the EDC ice core[12]; **h**, δD composition of ice in the EDC ice core[18]. Marine and ice-core records plotted on their own timescales. Marine Isotope Stages and sub-Stages and Antarctic Isotope Maxima (AIMs) are indicated. Dashed lines denote ODP 983–EDC correlation of events. Horizontal bars indicate estimates of interglacial duration (see main text).

of significant millennial-scale variability is difficult to constrain from these records. At the last glacial inception, sea level started falling ~3 kyr before the onset of significant bipolar-seesaw variability. Transient simulations with the CLIMBER-2 intermediate-complexity model with interactive ice-sheets show a faster increase in inland-ice area and volume at lower insolation minima compared to moderate minima[5]. The more subdued MIS19 insolation forcing suggests that, if anything, the initial ice extension towards the coast would have been slower than in MIS5e–5d, so the value of 3 kyr may be treated as a minimum. Applying the same response phasing to MIS19 places the timing of glacial inception ~775.5 kyr BP in EDC, or ~777.5 kyr BP in ODP 983, leading to an approximate interglacial duration of 12.5–10.5 kyr. The insolation minimum at that time was similar to the modern, but CO_2 concentrations were below preindustrial levels: combined chronological and experimental uncertainties suggest a CO_2 range of 240 ± 5 ppmv (Supplementary Fig. S4). Taking the MIS1–MIS19c analogy to its logical conclusion implies that the current interglacial would be nearing its end, provided that CO_2 concentrations were 240 ± 5 ppmv. Thus the question over the hypothetical timing of the next glacial inception continues to hinge on whether preindustrial CO_2 levels of 280 ppmv were 'natural' or had an anthropogenic component. If the comparison with MIS19c extends beyond a simple astronomical analogy (that is,

insolation is sufficient to predict CO_2 and climate evolution), it suggests that Holocene CO_2 concentrations should have fallen to levels below 250 ppmv by today, in line with Ruddiman's hypothesis[10]. The alternative to this is that CO_2 and insolation do not necessarily covary, as for example during MIS15c, which may represent a more appropriate 'carbon-cycle analogue' for the Holocene, unless its CO_2 evolution was a function of its slow deglaciation[11].

The empirical evidence from MIS19c converges with those modelling results[4,6] indicating a CO_2 threshold of 240 ± 5 ppmv for glacial inception, and suggests that ice-sheets reached sufficient size to extend to North Atlantic coasts, despite the subdued insolation forcing. Moreover, it shows that glacial inception occurred near the insolation minimum at 777 kyr BP, much earlier than the obliquity minimum at 765 kyr BP, unless ice-core and marine timescales are biased towards older ages by 10–12 kyr, which exceeds their chronological uncertainties. The duration of MIS19c, therefore, is at variance with the notion that at times of low eccentricity over the past 800 kyr interglacial length is about half an obliquity cycle[7,9,16]. The protracted length of the MIS11c and also MIS17 interglacials (Supplementary Fig. S5) may instead be related to obliquity maxima and precession minima being nearly opposite in phase rather than a result of weak eccentricity–precession forcing, which does not characterize MIS17.

In summary, the MIS19 evidence helps narrow the debate over the natural length of the current interglacial in terms of natural preindustrial CO_2 levels, rather than in terms of half-precession versus half-obliquity cycles. Although verification of an imminent glacial inception will elude us at current CO_2 concentrations, it is important to reiterate that the current insolation forcing and lack of new ice growth mean that orbital-scale variability will not be moderating the effects of anthropogenically induced global warming.

Methods

MIS1 and MIS19c were synchronized by aligning the precession minima/summer insolation maxima at 11 kyr BP and 788 kyr BP, so that today corresponds to 777 kyr BP. An almost identical solution emerges by aligning the obliquity maxima at 10 kyr BP and 788 kyr BP, so that today corresponds to 778 kyr BP. Similarly, MIS1 and MIS15c were synchronized by aligning the precession minima/summer insolation maxima at 11 kyr BP and 621 kyr BP, so that today corresponds to 610 kyr BP in MIS15c. An almost identical solution emerges by aligning the obliquity maxima at 10 kyr BP and 621 kyr BP, so that today corresponds to 611 kyr BP. Alignment of terminations was not used because ice-core and marine timescales may evolve compared to astronomical timescales.

ODP site 983 (60°23′ N, 23°38′ W; 1985 m water depth) is located on Gardar Drift, North Atlantic. Analytical methods for the records presented here are reported in the original publications[25–27]. The ODP 983 timescale[25] is based on tuning the $\delta^{18}O_{benthic}$ record to an ice-volume model, which is similar to the chronology of the LR04 $\delta^{18}O_{benthic}$ stack[28], but not entirely independent with respect to the timing of glacial inception as it assumes fixed lags between insolation forcing and ice-volume response. Nevertheless, the timing of the onset of bipolar-seesaw variability in ODP 983 is within the uncertainties of the EDC3 timescale[18], which crucially is independent of assumptions regarding ice-volume changes.

Cross-correlation analysis, using the program Analyseries of Didier Paillard, was carried out on the $\delta^{18}O_{benthic}$ and $\delta^{18}O_{planktonic}$ records of (1) ODP 983 for the interval 763.5–774.5 kyr BP, and (2) two MIS3 sequences, MD95-2042 and MD01-2444, on the Portuguese margin for the interval 36–48 kyr (refs 20,21).

Received 23 May 2011; accepted 28 November 2011; published online 8 January 2012

References

1. Archer, D. & Ganopolski, A. A movable trigger: Fossil fuel CO_2 and the onset of the next glaciation. *Geochem. Geophys. Geosyst.* **6,** Q05003 (2005).
2. Loutre, M. F. & Berger, A. Future climatic changes: are we entering an exceptionally long interglacial? *Climatic Change* **46,** 61–90 (2000).
3. Vettoretti, G. & Peltier, W. R. Sensitivity of glacial inception to orbital and greenhouse gas climate forcing. *Quat. Sci. Rev.* **23,** 499–519 (2004).
4. Cochelin, A-S., Mysak, L. A. & Wang, Z. Simulation of long-term future climate changes with the green McGill paleoclimate model: The next glacial inception. *Climatic Change* **79,** 381–401 (2006).
5. Calov, R., Ganopolski, A., Kubatzki, C. & Claussen, M. Mechanisms and time scales of glacial inception simulated with an Earth system model of intermediate complexity. *Clim. Past* **5,** 245–258 (2009).
6. Kutzbach, J. E., Ruddiman, W. R., Vavrus, S. J. & Philippon, G. Climate model simulation of anthropogenic influence on greenhouse-induced climate change (early agriculture to modern): The role of ocean feedbacks. *Climatic Change* **99,** 351–381 (2010).
7. Vettoretti, G. & Peltier, W. R. The impact of insolation, greenhouse gas forcing and ocean circulation changes on glacial inception. *Holocene* **21,** 803–817 (2011).
8. Kukla, G. J., Matthews, R. K. & Mitchell, J. M. The end of the present interglacial. *Quat. Res.* **2,** 261–269 (1972).
9. Masson-Delmotte, V. *et al.* Past temperature reconstructions from deep ice-cores: Relevance for future climate change. *Clim. Past* **2,** 145–165 (2006).
10. Ruddiman, W. F. The early anthropogenic hypothesis: Challenges and responses. *Rev. Geophys.* **45,** RG4001 (2007).
11. Ruddiman, W. F., Kutzbach, J. E. & Vavrus, S. J. Can natural or anthropogenic explanations of late-Holocene CO_2 and CH_4 increases be falsified? *Holocene* **21,** 865–879 (2011).
12. Lüthi, D. *et al.* High-resolution carbon dioxide concentration record 650,000–800,000 years before present. *Nature* **453,** 379–382 (2008).
13. Loulergue, L. *et al.* Orbital and millennial-scale features of atmospheric CH_4 over the past 800,000 years. *Nature* **453,** 383–386 (2008).
14. Tzedakis, P. C. *et al.* Interglacial diversity. *Nature Geosci.* **2,** 751–755 (2009).
15. Rohling, E. J. *et al.* Comparison between Holocene and Marine Isotope Stage-11 sea-level histories. *Earth Planet. Sci. Lett.* **291,** 97–105 (2010).
16. EPICA community members, Eight glacial cycles from an Antarctic ice core. *Nature* **429,** 623–628 (2004).
17. Tzedakis, P. C. The MIS 11—MIS 1 analogy, southern European vegetation, atmospheric methane and the early anthropogenic hypothesis. *Clim. Past* **6,** 131–144 (2010).
18. Jouzel, J. *et al.* Orbital and millennial antarctic climate variability over the past 800,000 years. *Science* **317,** 793–796 (2007).
19. Stocker, T. F. & Johnsen, S. J. A minimum thermodynamic model for the bipolar seesaw. *Paleoceanography* **18,** PA1087 (2003).
20. Shackleton, N. J., Hall, M. A. & Vincent, E. Phase relationships between millennial-scale events 64,000–24,000 years ago. *Paleoceanography* **15,** 565–569 (2000).
21. Margari, V. *et al.* The nature of millennial-scale climate variability during the past two glacial periods. *Nature Geosci.* **3,** 127–133 (2010).
22. Hodell, D. A., Evans, H. F., Channell, J. E. T. & Curtis, J. H. Phase relationships of North Atlantic ice rafted debris and surface sediment proxies during the last glacial period. *Quat. Sci. Rev.* **29,** 3875–3886 (2010).
23. Skinner, L. C., Elderfield, H. & Hall, M. in *Past and Future Changes of the Ocean's Meridional Overturning Circulation: Mechanisms and Impacts* (eds Schmittner, A., Chiang, J. & Hemming, S. R.) 197–208 (AGU Monograph, 2007).
24. Thompson, W. G. & Goldstein, S. L. A radiometric calibration of the SPECMAP timescale. *Quat. Sci. Rev.* **25,** 3207–3215 (2006).
25. Channell, J. E. T. & Kleiven, H. F. Geomagnetic palaeointensitites and astrochronological ages for the Matuyama–Brunhes boundary and the boundaries of the Jaramillo Subchron: Palaeomagnetic and oxygen isotope records from ODP Site 983. *Phil. Trans. R. Soc. Lond. Ser. A* **358,** 1027–1047 (2000).
26. Kleiven, H. F., Hall, I. R., McCave, I. N., Knorr, G. & Jansen, E. Coupled deep-water flow and climate variability in the middle Pleistocene North Atlantic. *Geology* **39,** 343–346 (2011).
27. Channell, J. E. T., Hodell, D. A., Singer, B. S. & Xuan, C. Reconciling astrochronological and $^{40}Ar/^{39}Ar$ ages for the Matuyama–Brunhes boundary and late Matuyama Chron. *Geochem. Geophys. Geosyst.* **11,** Q0AA12 (2010).
28. Lisiecki, L. E. & Raymo, M. E. A Pliocene–Pleistocene stack of 57 globally distributed benthic $\delta^{18}O$ records. *Paleoceanography* **20,** PA1003 (2005).
29. Laskar, J. *et al.* A long term numerical solution for the insolation quantities of the Earth. *Astron. Astrophys.* **428,** 261–285 (2004).
30. Huybers, P. Early Pleistocene glacial cycles and the integrated summer insolation forcing. *Science* **313,** 508–511 (2006).

Acknowledgements

We are grateful to members of the Past Interglacials (PIGS) working group of the Past Global Changes (PAGES) project, especially B. Thompson, A. Landais and J. McManus, for discussions. We thank R. Preece and M. Maslin for comments on the manuscript and D. Oppo for providing ODP980 data. H.F.K. acknowledges support from the Research Council of Norway, AMOCINT project; P.C.T. acknowledges support from the UK Natural Environment Research Council. This is a contribution to the PAGES PIGS project.

Author contributions

All authors contributed to the ideas developed in the paper. P.C.T. wrote the paper, with contributions from the other authors.

Additional information

The authors declare no competing financial interests. Supplementary information accompanies this paper on www.nature.com/naturegeoscience. Reprints and permissions information is available online at http://www.nature.com/reprints. Correspondence and requests for materials should be addressed to P.C.T.